Tunable active acoustic metamaterials

Bogdan-Ioan Popa,* Lucian Zigoneanu, and Steven A. Cummer†
Department of Electrical and Computer Engineering, Duke University, Durham, North Carolina 27708, USA
(Received 1 May 2013; revised manuscript received 2 July 2013; published 16 July 2013)

We describe and demonstrate an architecture for active acoustic metamaterials whose effective material parameters can be tuned independently over a wide range of values, including negative material parameters. The approach is demonstrated experimentally through the design and measurement of two types of unit cells that generate metamaterials in which either the effective density or bulk modulus can be tuned. We show that these unit cells achieve negative refraction, negative effective mass density, significantly nonunity bulk modulus, and are suitable for the design of negative refraction media and media with tunable gain and absorption. In this architecture, a transducer senses the pressure wave incident on the metamaterial and an electronic circuit manipulates the electric signal produced and drives a second transducer that creates the acoustic response consistent with the desired effective material parameters. The electronics between the two transducers allows easy dynamic tuning of these parameters. We show that this approach can be applied to both broadband and narrow band designs.

DOI: 10.1103/PhysRevB.88.024303 PACS number(s): 43.20.−f, 43.60.Fg, 46.40.Cd

I. INTRODUCTION

The development of advanced design techniques in acoustics such as transformation acoustics[1–4] sparked increased interest in the research of complex engineered fluidlike materials (called metamaterials or metafluids) capable of implementing the remarkable devices prescribed by these techniques. The focus has been on obtaining passive metamaterial structures with effective material parameters characterized by negative values,[5–14] high anisotropy,[15–23] enhanced absorption,[24] having required gradients,[21,25–28,30] or the acoustic analog of the unique electromagnetic properties of graphene.[31] In turn, the increased range of material parameters made available by these structures and the close resemblance to their electromagnetic counterparts meant that novel acoustic devices became possible, such as various acoustic gradient lenses,[21,25–28,30] invisibility cloaks,[20,22] or novel absorbers.[24]

Passive acoustic metamaterials extend the range of achievable parameters in naturally occurring materials. However, they have limitations. For example, for acoustics in air, subunity relative material parameters needed for high-performance acoustic lenses or transformation acoustics devices can only be achieved passively in resonant structures that are not only narrow band but also lossy and, consequently, have limited applications. Moreover, effective material parameters are correlated in passive materials, therefore, one has a limited degree of freedom in controlling them independently. For instance, a passive metafluid in which the effective bulk modulus is considerably larger than that of the background fluid, necessarily contains stiff inclusions that occupy a significant volume. Stiff materials are usually denser, which increases the effective mass density as well. Therefore, large effective bulk moduli typically imply larger effective densities. This is an unwanted consequence in many applications, such as acoustic lensing, because it causes poor matching between the background fluid and the lens.[21,27,30] A notable exception is a new type of metamaterial structure[32] that can be made stiff and light at the same time; however, such an approach is harder to adopt in applications in which the background fluid has low density, as is the case of air.

In contrast, active metamaterials do not suffer from these limitations, because their acoustic response is manipulated through electronically controlled elements and not through material inclusions. Therefore, active metamaterials can achieve a much wider range of effective parameters than their passive counterparts. The advantage of active complex materials has been acknowledged by others.[33,34] Moreover, a recent experiment of an active cell consisting of an actuated cavity has shown that, in principle, mass density can be controlled actively.[34] However, no systematic way of designing active metamaterials has been reported yet.

The goal of this work is to show how active acoustic metamaterials can be systematically designed to achieve desired material parameters. We employ an idea first proposed for electromagnetics[35] and whose efficacy was demonstrated experimentally in the realization of negative parameter electromagnetic metamaterials[36] and nonreciprocal media.[37] More specifically, a transducer is used to sense the incident pressure field, p_i, impinging on the unit cell that generates the metafluid [see Fig. 1 (top)]. Electronic circuits characterized by the impulse response function G manipulate the resulting electrical signal, v_i, generate a signal v_o, which, in turn, drives a second transducer that generates the desired acoustic cell response represented by p_r^{act} and p_t^{act}.

Throughout the paper we use the term architecture to refer to this style of designing active cells that employ sensing and driven transducers, electronics, and their support structures. This approach has several advantages compared to the electromagnetics case. The most important is that acoustic waves have very low group velocities compared to the speed of modern electronics. Consequently, the active response of the metamaterial can be made almost instantaneous. In addition, the vast majority of acoustic applications require frequencies lower than 100 MHz for which high-quality, compact electronic components and design tools are ubiquitous.

Our purpose here is to demonstrate experimentally various active unit cells with interesting responses hard to obtain otherwise. Specifically, we design a unit cell of tunable effective mass density (of negative and positive values) capable of negative refraction, and, despite it being resonant, having

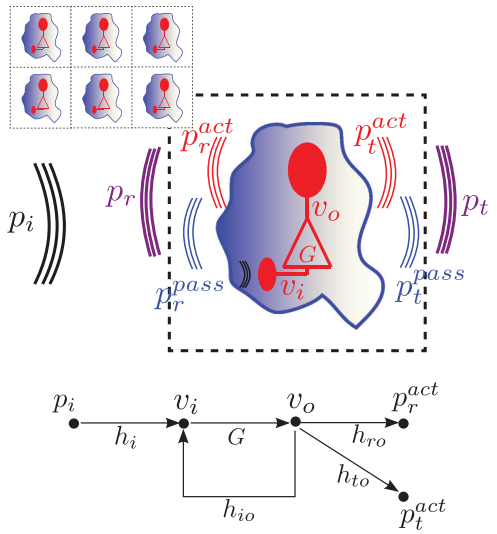

FIG. 1. (Color online) Metafluid made of active unit cells. Top: the unit cell contains the passive components (blue, irregular shape) that helps the metafluid pictured in the inset maintain its structural integrity. The passive components hold together the active elements: the sensing (red, small ellipse) and driven (red, big ellipse) transducers and the electronics used to manipulate the cell response (red triangle) to an incident pressure wave, p_i. The reflected, p_r, and transmitted, p_t, waves are a superposition of the passive and active contributions. Bottom: flow graph describing the cell behavior.

low loss or even gain. The second cell presented here has broadband bulk modulus tunable over a wide range. In both cases, the untuned material parameter (modulus for the former, density for the latter) stays relatively unchanged regardless of the tuned parameter value.

II. CONTROLLING MASS DENSITY AND BULK MODULUS

To better understand how the fluid mass density and bulk modulus can be manipulated, it is advantageous to quantify the response of the fluid to acoustic excitation in terms of multipole sources generated inside the fluid by the external excitation. Under the small displacements approximation for which the linear acoustic wave equation is derived, only the monopole and dipole sources will be non-negligible. In analogy with electromagnetics, we can model an inhomogeneous and anisotropic fluid as a periodic array of compact monopole, Q, and dipole, $\mathbf{q}$, sources embedded in an isotropic, homogeneous, incompressible, and nonviscous background fluid characterized by mass density, ρ_b, and bulk modulus, B_b. The Helmholtz equation governing the propagation of acoustic waves through it is

$$\nabla \cdot (\nabla p - \mathbf{q}) + k_b^2 p = Q, \tag{1}$$

where the wave vector is written in terms of angular frequency as $k_b^2 = \omega^2 \rho_b / B_b$. Assuming that the dipole sources have a linear response to the local force density, $\mathbf{q} \equiv \overline{\overline{m}} \nabla p$, while the monopole sources have a linear response to the local flow of force density, $Q \equiv n k_b^2 p$, where the tensor $\overline{\overline{m}}$ and scalar n are the proportionality factors, the equation above can be written

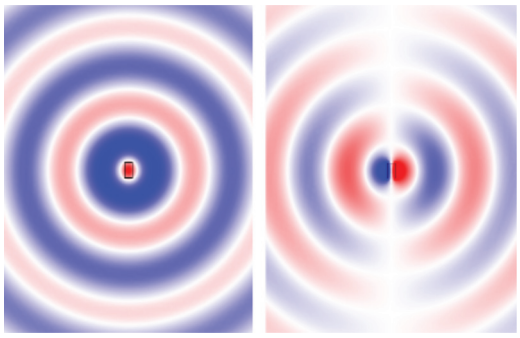

FIG. 2. (Color online) Acoustic fields produced by monopole (left, $Q \neq 0$, $\mathbf{q} = 0$) and dipole (right, $Q = 0$, $\mathbf{q} = \hat{\mathbf{x}} q \neq 0$, where $\hat{\mathbf{x}}$ is the unit vector in the horizontal direction) sources.

$$\nabla \cdot \left(\overline{\overline{\rho}}_{\text{eff}}^{-1} \nabla p\right) + \frac{k_b^2}{B_{\text{eff}}} p = 0, \tag{2}$$

where $B_{\text{eff}} \equiv (1-n)^{-1}$ and $\overline{\overline{\rho}}_{\text{eff}} \equiv (I_3 - \overline{\overline{m}})^{-1}$ are essentially the effective bulk modulus and, respectively, mass density tensor of our modeled fluid relative to the material parameters of the background fluid.

The above expressions of the effective material parameters B_{eff} and $\overline{\overline{\rho}}_{\text{eff}}$ reveal that we can control the mass density inside a metamaterial through inclusions whose responses mimic the behavior of dipole sources and the bulk modulus through inclusions that behave as monopole sources. Figure 2 shows the fields produced by such sources obtained in a numerical simulation performed with the acoustics module of COMSOL MULTIPHYSICS, a commercial finite element method solver of the acoustic wave equation (1). We note that the fields of a dipole are very similar to the strongly asymmetric pressure fields created by a planar vibrating membrane: as the membrane pushes the fluid on one of its sides, it pulls the fluid on the other side, therefore, the acoustic pressure fields created on the two sides will have opposite signs.

This is an intuitive explanation of why periodic arrays of membranes[11] and perforated plates[16,25] can be used to control the mass density in a metamaterial. Helmholtz cavities with their symmetric response, on the other hand, create acoustic fields similar to a monopole source, and, therefore, can be used to control the bulk modulus in a metamaterial.[10] Next we use this physical insight to design active metafluids.

III. DESIGN APPROACH

A widely used procedure to design two-dimensional (2D) or three-dimensional (3D) metamaterial unit cells is to perform a series of one-dimensional (1D) numerical simulations and/or measurements of plane waves interacting with a single metamaterial unit cell, modeled as a two-port device characterized by an S-parameter matrix, and record the reflected and transmitted waves. Inverting the reflection (S_{11}) and transmission (S_{21}) coefficients thus obtained, one can recover the effective parameters of the metafluid generated by the cell.[39] We take here the same approach. We focus on metafluid cells whose S parameters satisfy $S_{11} = S_{22}$ and $S_{21} = S_{12}$ and, therefore, the metafluid can be described in terms of anisotropic mass

density and isotropic bulk modulus. The general situation in which the metafluid cannot be described in such simple terms (for example nonreciprocal media) can, however, be treated using the same approach, but the analysis is more involved. All quantities are expressed in frequency domain throughout the paper, and, as such, are functions of frequency.

Figure 1 (top) sketches the behavior of the cell in a 1D setting. The passive response of the cell is represented by the the pressure waves transmitted (p_t^{pass}) and reflected (p_r^{pass}) by the physical structure of the cell. In addition, the cell has an active response created by the driven transducer in the direction of the reflected and transmitted waves represented by p_r^{act} and, respectively, p_t^{act}. The overall reflected (p_r) and transmitted (p_t) waves will be the superposition of the passive and active responses, and the S parameters are given by

$$\begin{aligned} S_{11} &\equiv p_r/p_i = S_{11}^{\text{pass}} + h_{11}^{\text{act}}, \\ S_{21} &\equiv p_t/p_i = S_{21}^{\text{pass}} + h_{21}^{\text{act}}, \end{aligned} \tag{3}$$

where $S_{11}^{\text{pass}} \equiv p_r^{\text{pass}}/p_i$, $S_{21}^{\text{pass}} \equiv p_t^{\text{pass}}/p_i$, $h_{11}^{\text{act}} \equiv p_r^{\text{act}}/p_i$, and $h_{21}^{\text{act}} \equiv p_t^{\text{act}}/p_i$. The passive components S_{11}^{pass} and S_{21}^{pass} are determined by the cell geometry and controlling them was discussed elsewhere.[5–23] The focus of this paper is on the two active terms h_{11}^{act} and h_{21}^{act} and how they can be used to manipulate S_{11} and S_{21}, and through them, the metafluid effective material parameters.

Assuming the active response is linear, we can quantify the behavior of the active cell using a set of four transfer functions. They describe the behavior of the sensing transducer ($h_i \equiv v_i/p_i$) and driven transducer in the direction of the reflected ($h_{ro} \equiv p_r^{\text{act}}/v_o$) and transmitted ($h_{to} \equiv p_t^{\text{act}}/v_o$) waves, and the coupling between the driven and sensing transducers (h_{io}), i.e., if the voltage on the driven transducer is v, then the voltage measured on the sensing transducer as a result of this excitation alone is $h_{io}v$.

The relations between the transfer functions described above are summarized in the flow graph outlined in Fig. 1 (bottom). These allow us to compute the active contribution to the S parameters associated with the unit cell by applying Mason's formula[38] on the graph. We obtain

$$h_{11}^{\text{act}} \equiv \frac{p_r^{\text{act}}}{p_i} = \frac{h_i G h_{ro}}{1 - h_{io}G}, \quad h_{21}^{\text{act}} \equiv \frac{p_t^{\text{act}}}{p_i} = \frac{h_i G h_{to}}{1 - h_{io}G}. \tag{4}$$

The above equations show that we can control the response of the cell by properly designing the electronic circuit whose transfer function is G. In addition, we have some control over the values of h_{ro} and h_{to} through our choice of transducer elements. For example, as explained in the previous section, if the transducer is an actuated planar membrane, the sound produced in one direction is 180° out of phase with respect to the sound produced in the other direction, and $h_{ro} = -h_{to}$. Consequently, it behaves as a dipole, and, as such, it is an efficient element to manipulate the effective mass density of the cell. On the other hand, two such membranes of inverted polarities generate an in-phase response for which $h_{ro} = h_{to}$. The cell behaves as a monopole and, thus, will have a tunable effective bulk modulus.

These two cases will be demonstrated in the experiments described in the following sections. In general, the relation between h_{ro} and h_{to} is arbitrary. More importantly, the phase difference between them can be controlled through an electric circuit connecting the two transducers. Therefore, both the bulk modulus and mass density can be controlled at the same time.

To summarize, a typical design approach consists in choosing the transducer elements that control the required material parameters (mass density and/or bulk modulus) and, through that, the ratio h_{ro} to h_{to}. Then, we design the cell supporting structure, i.e., S_{11}^{pass} and S_{21}^{pass}, followed by measurements of the transfer functions $h_i h_{or}$, $h_i h_{ot}$, and h_{io}. Based on these measurements, we then design the cell electronics, G, that produce the desired cell response/cell effective material parameters using Eqs. (3) and (4).

IV. STABILITY

As with any active system, stability issues have to be taken into account in the design. In our case there are two causes of potential instability.

The first comes from the intracell feedback loop between the driven and sensing transducers. In general, the cell is unconditionally stable as long as all the poles of h_{11}^{act} and h_{21}^{act} given by Eqs. (4) have negative real values. For example, a cell featuring low feedback characterized by $|h_{io}G| < 1$ has no poles and, therefore, is unconditionally stable.

A second cause of instability comes from the intercell coupling in a bulk metafluid. This type of instability can be efficiently analyzed using S-parameter techniques. As pointed out above, measurements of cell S parameters in experiments and numerical simulations have been for a long time part of popular techniques used to design acoustic and electromagnetic metamaterials, because they can be inverted to yield the effective material parameters of the bulk metamaterial/metafluid. It is thus natural to use them to characterize the stability of the bulk metamaterial. More specifically, to have an unconditionally stable metamaterial, the Edwards-Sinsky stability parameter must be greater than unity[41]

$$\frac{1 - |S_{11}|^2}{|S_{11} - S_{11}^* \Delta| + |S_{21}|^2} > 1, \tag{5}$$

where S_{11} and S_{21} are given by Eqs. (3) and $\Delta = S_{11}^2 - S_{21}^2$. Recall that in this paper we are interested in metafluids that can be described in terms of anisotropic mass density and scalar bulk modulus, consequently, the above equation assumes that the unit cell is designed such that $S_{11} = S_{22}$ and $S_{21} = S_{12}$. Stability analysis of nonreciprocal metafluids easily achievable using the active cell architecture described above would need to use the Edwards-Sinsky stability parameter corresponding to an arbitrary S-parameter matrix.

Equation (5) assures that the metafluid is always stable regardless of its environment. In practice, however, this constraint is unnecessarily restrictive, as particular applications require stability only for a certain environment modeled as impedances Z_1 and Z_2 connected to the two-port representation of the unit cell. We define the reflection coefficients associated to the environmental impedances as $\Gamma_i = (Z_i - Z_b)/(Z_i + Z_b)$, where $i \in \{1,2\}$ and $Z_b \equiv \sqrt{B_b \rho_b}$ is the impedance of the background fluid to which the cell S-parameter matrix is normalized. Then the metafluid stability condition corresponding to the environment described by Z_1

and Z_2 can be written

$$\left|\frac{S_{11}-\Delta\Gamma_i}{1-S_{11}\Gamma_i}\right|<1. \tag{6}$$

For instance, a lens made of a one unit cell thick metafluid structure placed reasonably away from scattering objects (i.e., $Z_i = Z_b$, thus, $\Gamma_i = 0$) has to be made of unit cells characterized by $|S_{11}| < 1$.

V. NEGATIVE REFRACTION WITH A NEGATIVE DENSITY METAFLUID

We demonstrate the design procedure described in the preceding sections with two examples. The first one is the design of a homogeneous metafluid in air ($k_b = k_0$) characterized by negative refraction around 2500 Hz.

As pointed out in the past,[42,43] negative refraction does not necessarily imply a negative index of refraction. Instead it means that, assuming $\exp(j\omega t)$ time variation, the phase of S_{21} must be positive and with no 360° phase wraps occurring. Obtaining this feature is our design goal.

For its simplicity, we choose for the driven transducer a piezoelectric (PZT) membrane produced by PUI Audio Inc., whose vibration is controlled through a voltage signal applied on it. As pointed out above, the membrane is characterized by $h_{or} = -h_{ot}$. Depending on how it is mounted, the membrane resonates at a frequency below 10 kHz. Since at resonance its response has maximum intensity, our design goal is to mount it such that its resonance is in the band of interest 2000 Hz to 3000 Hz. For this reason, we chose the diameter of the membrane region free to vibrate to be 3.8 cm.

The sensing transducer is a unidirectional electret from ICC Intervox (6 mm diameter, 5 mm height) connected to a Stanford Research Systems SR560 bandpass amplifier whose gain is set to 500, and cutoff frequencies are set to 1000 Hz and 3000 Hz. Since the transmission coefficient S_{21} is given by Eqs. (3), and because the control of this parameter comes mostly from the h_{21}^{act} component, we design the unit cell to have S_{21}^{pass} as close to zero as possible. Consequently, the PZT and its supporting plastic frame are designed to block the incoming sound and, thus, minimize S_{21}^{pass}. They are presented in Fig. 3 (top). The electret is mounted in a hole drilled in the plastic frame using a vibration damping felt fabric. This minimizes the coupling between the sensing and driven transducers due to the vibrations transmitted directly through the solid frame, and leads to a significantly reduced h_{io}, the term responsible for intracell instability.

Having the transducers and geometry of the unit cell chosen, we measure the transfer functions appearing in Eqs. (4) in the 1D rectangular waveguide shown in Fig. 3. The cell dimensions are chosen so that the cell is smaller than a quarter of a wavelength in the 2000 Hz to 3000 Hz, thus, it can be described in terms of effective material parameters. With the dimensions given in Fig. 3, this constraint is satisfied for angles of incidence of less than 30°, where normal incidence (0°) corresponds to the situation in which the direction of propagation is perpendicular on the PZT membrane. The rigid waveguide walls simulate periodic boundaries and normal incidence, and, thus, measurement of one cell is equivalent

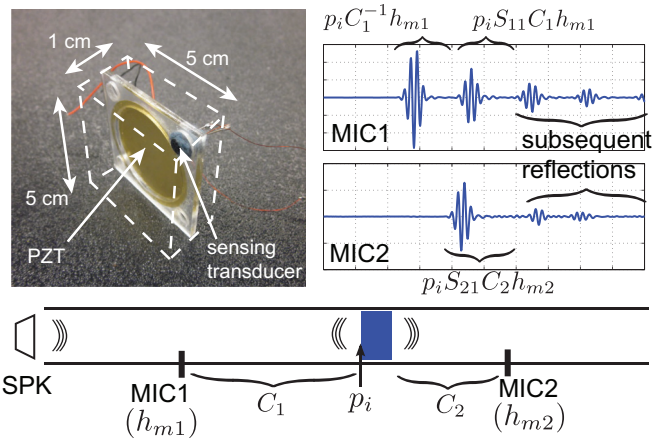

FIG. 3. (Color online) Active unit cell and experimental setup used to measure the cell properties. Top, left: photograph of the active cell; bottom: The properties of metamaterial cells are measured in a 1D waveguide excited at one end by a speaker (SPK) producing short Gaussian pulses. Two microphones, MIC1 and MIC2 (transfer functions, h_{m1} and h_{m2}), measure the time domain waveforms inside the waveguide. The transfer functions of the two sections of waveguide between the cell and microphones are labeled C_1 and C_2. Top, right: Various components of the time domain waveforms measured by MIC1 and MIC2 are annotated in terms of transfer functions and incident wave pulse p_i at cell boundary.

to measuring an infinitely wide, one-cell-thick metafluid, on which the acoustic wave impinges perpendicularly.

The cell is placed in the middle of the waveguide with the 1 cm side parallel to the direction of propagation. Two microphones, labeled MIC1 and MIC2, placed $l_1 = 60$ cm in front and, respectively, $l_2 = 40$ cm behind the cell measure the pressure field inside the waveguide. The microphone transfer functions are denoted by h_{m1} and, respectively, h_{m2} and represent the ratio of the voltages generated by the microphones to the sound pressure inside the waveguide. The impulse response of the waveguide sections between the microphones and the unit cell are represented by C_1 and C_2. Ideally, $C_1 = \exp(-jk_0l_1)$ and $C_2 = \exp(-jk_0l_2)$; however, in practice the wave is attenuated because sound energy escapes through the waveguide walls of finite thickness.

The sound source, either the PZT membrane or a speaker mounted at one end of the waveguide (labeled SPK in Fig. 3), produces short Gaussian envelope pulses centered on frequency f_0. The pulses are short enough so that multiple reflections due to the cell PZT or waveguide speaker can be easily isolated by time windowing the measured waveforms.

To measure h_{io}, a voltage v_{pzt} is applied on the PZT membrane via a National Instruments data acquisition card (NIDAQ). The signal measured on the sensing transducer is recorded by the same NIDAQ. If we denote it v_1, it follows that

$$h_{io} = \frac{v_1}{v_{\text{pzt}}}. \tag{7}$$

The signal measured in this case by MIC1 is $v_2 = v_{\text{pzt}}h_{or}C_1h_{m1}$. Two more measurements are then needed to compute h_ih_{or}. The first is when the cell is replaced by a perfect reflector, i.e., a solid block of metal whose reflection

coefficient can be approximated to 1 across the frequencies of interest. In this case, the waveguide speaker sends a sound pulse p_i towards the reflector, and the signal reflected back towards the speaker is measured by MIC1 as $v_3 = p_i C_1 h_{m1}$. For the second measurement, the unpowered cell is hit by the short pulse produced by SPK and the signal is measured by the cell sensing transducer as $v_4 = p_i h_i$. The reflected signal measured by MIC1 is $v_5 = p_i S_{11}^{\text{pass}} C_1 h_{m1}$. It follows that

$$h_i h_{or} = \frac{v_2 v_4}{v_3 v_{\text{pzt}}}. \tag{8}$$

The transfer functions given by Eqs. (7) and (8) allow us to compute h_{11}^{act} and h_{21}^{act} using Eqs. (4). Independently, the accuracy of these parameters can be verified by comparing them with those derived from Eqs. (3) in which S_{11}^{pass}, S_{21}^{pass}, S_{11}, and S_{21} are measured directly using a procedure employed in the past[21–23] and summarized below.

The S parameters associated with the passive cell are obtained from

$$S_{11}^{\text{pass}} = \frac{v_5}{v_3}, \quad S_{21}^{\text{pass}} = \frac{v_6}{v_7}, \tag{9}$$

where $v_6 = p_i S_{21}^{\text{pass}} C_2 h_{m2}$ and $v_7 = p_i C_2 h_{m2}$ are the first reflections measured at MIC2 with the unpowered cell and, respectively, inside the empty waveguide with the section of waveguide occupied by the cell removed. Note that the S parameters of the powered cell, S_{11} and S_{21}, are obtained using an identical procedure with v_5 and v_6 measured when the cell is powered.

Figure 4(a) shows the amplitudes of the transfer functions h_{io}, and $h_i h_{or}$. We note that $|h_{io}| < 0.2$, which means that the cell is stable as long as $|G| < 5$. Figures 4(b) and 4(c) show the complex (amplitude and phase) $h_{11}^{\text{act}} = -h_{21}^{\text{act}}$ obtained from Eq. (4), as well as h_{11}^{act} and h_{21}^{act} computed with Eqs. (3) from the S parameters measured with the powered and unpowered cell. The powered cell is obtained by directly connecting the output of the sensing transducer amplifier to the PZT membrane, i.e., $G = 1$. The measurements confirm our assumption that, for a vibrating membrane, h_{11}^{act} and h_{21}^{act} are 180° out of phase. Furthermore, the excellent match confirms the accuracy of the model presented above.

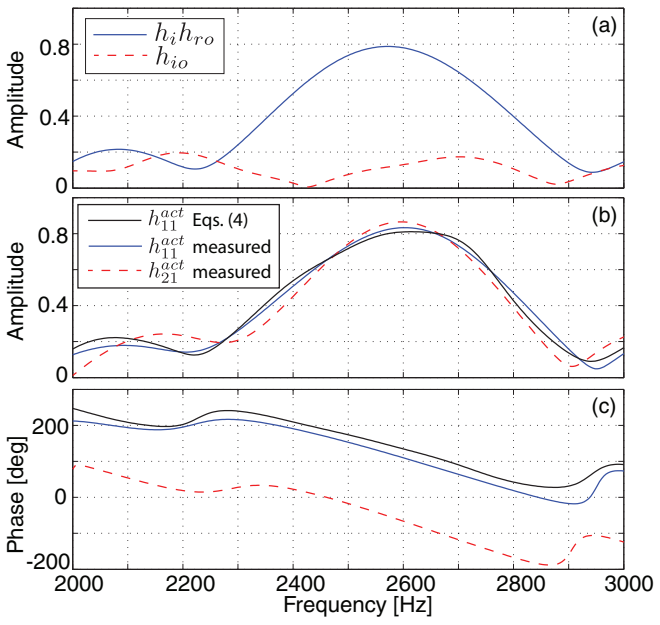

FIG. 4. (Color online) Measured transfer functions. Top: Complex amplitude of h_{io} and $h_i h_{ro}$ obtained from Eqs. (4), (7), and (8). Middle: Complex amplitude of h_{11}^{act} and h_{21}^{act} obtained directly from S-parameter measurements and Eqs. (3). Expected amplitude of h_{11}^{act} obtained from Eqs. (4); Bottom: Phase of h_{11}^{act} and h_{21}^{act} in the three cases listed above confirm the resonance of the PZT membrane in the expected band and the relation $h_{11}^{\text{act}} = -h_{21}^{\text{act}}$.

Unfortunately, $G = 1$ does not bring the phase of S_{21} to positive values (the maximum value of the phase reaches only $-22°$), thus, a metafluid made with these unit cells will still feature positive refraction. In order to make the phase of S_{21} positive, a positive phase shift of the sensed signal is required. For example, if $G = \exp(j50°)$, the phase of S_{21} becomes significantly greater than 0, as seen in Fig. 5(b). The expected S parameters, S_{11} and S_{21} [see Figs. 5(a) and 5(b)], together with the material parameters retrieved from them [see Figs. 5(c)–5(e)] are also shown as dashed curves.

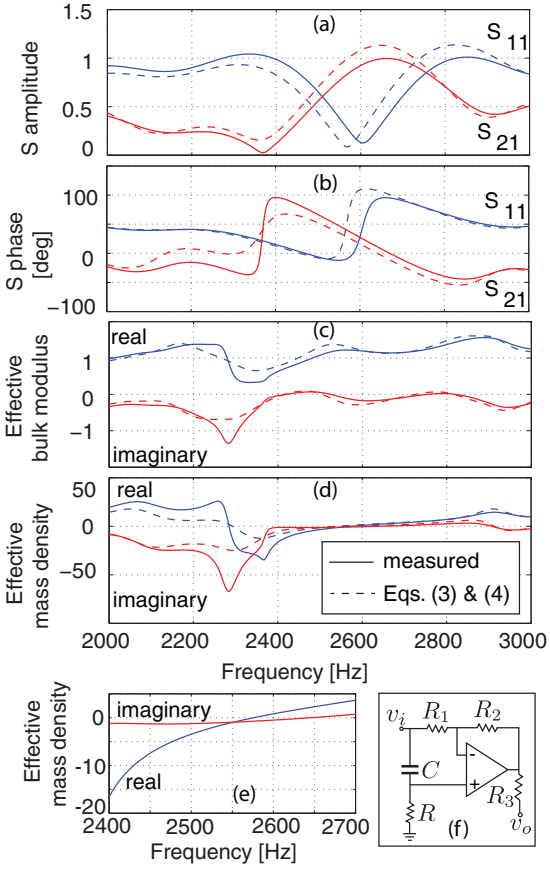

FIG. 5. (Color online) The measured (solid) and expected (dashed) active cell S-parameters amplitude (a) and phase (b) for the phase shifter shown in (f). Extracted effective material parameters normalized to the parameters of air show the bulk modulus (c) being close to unity in the entire band of 2000 Hz to 3000 Hz, while the effective density (d) has large negative values in the band of interest between 2400 Hz to 2500 Hz, in which the effective density is significantly negative and the homogeneization theory is valid; (e) Measured effective density in the 2400 Hz to 2700 Hz band; (f) Phase shifter schematic: OP27G op-amp, $C = 2.5$ nF, $R = 30$ KΩ, $R_1 = 820$ Ω, $R_2 = 1$ KΩ, $R_3 = 60$ Ω.

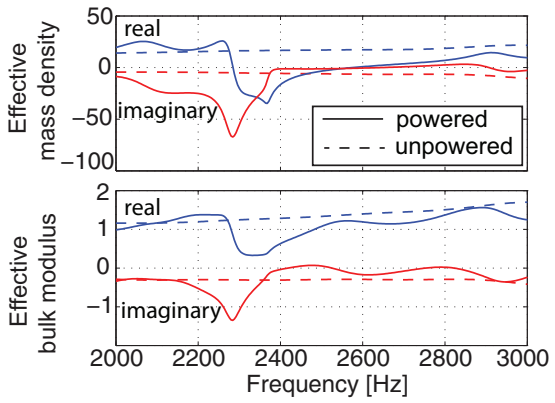

FIG. 6. (Color online) The measured effective material parameters of the powered (solid) and unpowered (dashed) cell. All material parameters are normalized to the parameters of air.

A phase shift of 50° can be achieved with the active all pass filter shown in the inset of Fig. 5(f). With the passive components presented in the figure caption, the phase shift varies between 60° and 40° in the band 2000 Hz to 3000 Hz, with the desired phase shift of 50° at ∼2500 Hz. This all pass filter was connected between the sensing transducer and the driven PZT. The measured active cell S parameters and effective material parameters extracted from them are plotted in Figs. 5(a)–5(e) as solid lines. The measurements were made with a narrow incident Gaussian pulse centered at 2500 Hz for which the signal to noise ratio is at least 30 dB in the band of interest.

We note the very good agreement between the measurements and predictions, which validates the design method. The phase of S_{21} becomes positive in the band between 2370 Hz and 2640 Hz, which means that negative refraction is achieved in this band.

To illustrate the contribution of the cell active response to the effective material parameters, Fig. 6 presents the effective bulk modulus and mass density of the powered and unpowered cell. As expected, the unpowered cell is characterized by almost constant material parameters. In contrast, the powered cell produces material parameters significantly different from those of the unpowered cell in the range of frequency in which the driven piezoelectric membrane is resonant and has a strong acoustic response.

The cell active response is controlled by the cell electronics (G). This provides a convenient way to dynamically tune the cell properties. Thus, the mass density is controlled by choosing the phase shift in the circuit shown in Fig. 5(f). For example, by increasing the phase shift in the all pass filter from 0 to 50° the effective density at 2400 Hz changed from approximately 0 to −15. This is easily obtained using electronically controlled components R and/or C.

Recall that the membrane producing the cell response acts as a good dipole radiator, therefore, as shown in Sec. II, we expect the cell to be characterized by a mass density significantly different from that of the background fluid, while the bulk modulus should remain mostly constant in the entire band. Indeed, the resonant nature of the PZT membrane is responsible for the measured large variation of the mass density. Strongly negative as well as positive values are obtained while the bulk modulus has a significantly smaller variation. The relatively small variation of the bulk modulus is mostly caused by the nonlocal phenomena similar to those producing the so-called antiresonance in electromagnetic metamaterials.[40]

We note that $|S_{11}|^2 + |S_{21}|^2$ varies between 0.99 and 0.75 in the useful band between 2400 Hz and 2500 Hz, in which the effective density is solidly negative. In this band the wavelength inside the metafluid is more than ten times bigger than the cell size, and, consequently, the homogenization theory that allows us to assign effective material parameters to the metafluid is valid. These values close to unity of $|S_{11}|^2 + |S_{21}|^2$ show that the active metafluid cell is very low loss compared to its passive counterparts. In addition, we note a ratio between the imaginary and real parts of the mass density varying between 0.07 at 2400 Hz where the relative density is −16.5, and 0.36 at 2500 Hz where the relative density becomes −3.4. Such small ratios have not been observed in passive resonant acoustic or electromagnetic metamaterials. In these latter cases, ratios significantly larger than 1 are typical close to the resonance. Moreover, we note that above ∼2650 Hz the cell becomes a gain medium as $|S_{11}|^2 + |S_{21}|^2 > 1$, and the imaginary part of the effective density becomes positive.

VI. BROADBAND CONTROL OF BULK MODULUS

In the previous example we designed a metafluid unit cell with a strong dipolelike response to incident sound waves. We showed that we can tune the effective mass density of such medium over a large range of values. Here we show that we can design metafluid cells in which we have similar control over the bulk modulus. If in the previous case the cell had a resonant nature due to our choice of driven transducer, here we show that this is not a physical limitation in active metamaterials by designing a broadband metafluid unit cell.

As pointed out in Sec. II, we control the bulk modulus in cells that have strong monopolelike responses. Helmholtz cavities, due to their symmetric response originating from a hole in the cavity, are such an example, but, unfortunately, these are resonant, therefore, narrow band elements. To avoid a resonant behavior, we use two broadband transducers produced by CUI Inc. Driven by the same signal, these produce a symmetric monopolelike response.

A photograph of the active cell is shown in Fig. 7 (inset) and uses the same architecture as the cell employed in the previous section. We use the same electret as before as our sensing transducer. The cell was designed to be as transparent as possible so that its effective material parameters are as close to those of the background medium. Hence, the frame holding the transducers has as little material as possible.

The h_{11}^{act} and h_{21}^{act} transfer functions of the active cell obtained from the measured S parameters of the powered and unpowered cell [see Eqs. (3)] when the electret's amplifier was directly connected to the driven transducer, i.e., $G = 1$, are shown in Fig. 7. They confirm that the cell acts as an acoustic monopole with a symmetric response, for which $h_{11}^{\text{act}} \approx h_{21}^{\text{act}}$.

Figure 8 shows the material parameters of the active cell in three instances. First, the solid lines mark the parameters of the passive, unpowered cell. They confirm effective bulk modulus and density close to those of air. The effective parameters of the powered cell ($G = 1$) show a broadband bulk modulus significantly larger than that of air. Bulk moduli smaller than

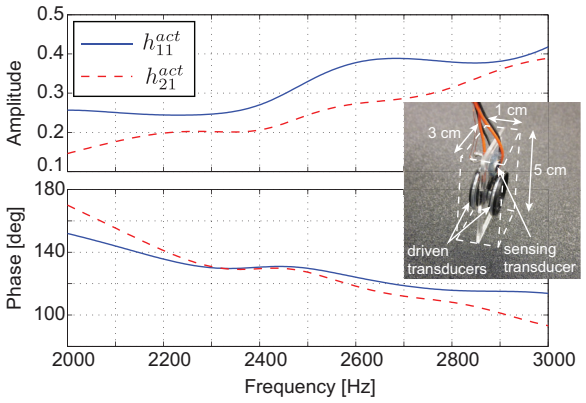

FIG. 7. (Color online) Symmetric response cell. Transfer functions h_{11}^{act} and h_{21}^{act} measured from S-parameter measurements and Eqs. (3) confirm that $h_{11}^{act} \approx h_{21}^{act}$. Note the broadband characteristics of the transfer functions. Inset: cell photo and dimensions. The sensing electret has a diameter of 6 mm and height of 5 mm, while the driven transducers have a diameter of 2.2 cm and a height of 5 mm.

what can be obtained with a broadband passive structure are also possible. A phase shift of 90° in the electronics, i.e., $G = \exp(j90°)$, generates the effective material parameters shown as dotted curves. We note the broadband bulk modulus whose value is noticeably below that of the passive cell.

Regardless of the bulk modulus value, the effective density remains virtually unchanged. This behavior is fundamentally hard to achieve in passive metafluids. A high value of the bulk modulus relative to that of the background fluid means that the cell must contain inclusions much stiffer than the background. Moreover, these inclusions must occupy a significant cell volume. Stiffer materials, however, are typically more dense, as the two properties are strongly correlated. The denser inclusions lead to an increase in the effective density. The active cell shown here does not suffer from this limitation because its response is controlled through the electronics and not through the material inclusions that compose the cell.

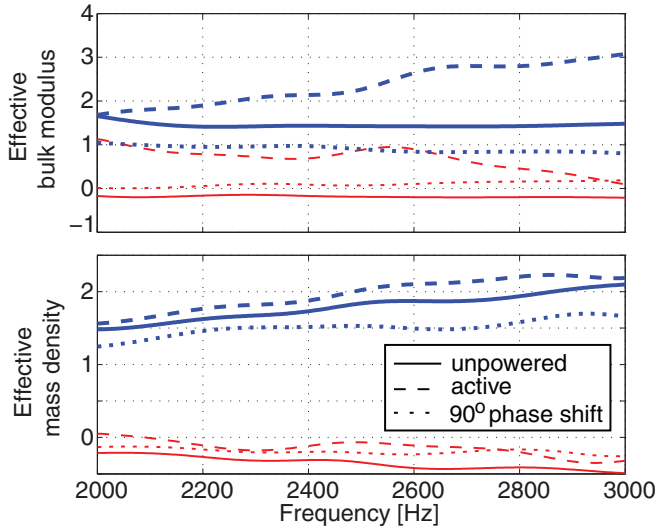

FIG. 8. (Color online) Measured effective material parameters normalized to the parameters of air in three cases: the unpowered cell ($G = 0$), active ($G = 1$) and calculated from Eqs. (3) and (4) assuming a phase shift of 90° [$G = \exp(j90°)$]. The bulk modulus is tuned over a large range of values by the phase shift. The real components are shown with thicker lines.

VII. CONCLUSION

We presented an active acoustic metafluid cell architecture that allows independent control of the effective material parameters of metafluids. In passive designs the effective bulk modulus is correlated with the mass density. This correlation can have adverse effects, for instance, it is the reason behind acoustic lenses being poorly matched with the surrounding background, especially when the background is air.[27,29,30]

Active metafluids solve this limitation. We showed in an experiment how the effective mass density can be tuned to have a wide range of positive and negative values, while the bulk modulus is kept almost constant in a wide frequency band. We showed in a different experiment that the bulk modulus can be tuned while the effective density is kept almost unchanged.

The architecture described here uses a sensing transducer to sample the incident acoustic field, electronics to manipulate the obtained electric signal, and a driven transducer to convert the resulting electric signal into acoustic energy. This approach allows one to control the metafluid response to the incident excitation and, implicitly, the metafluid effective material parameters. These parameters are tuned in a straightforward way by designing the cell electronics. In addition, the method enables loss control and even the design of gain media.

This idea has already been proven effective in designing active electromagnetic metamaterials. It is, however, more suitable for acoustics. Acoustic waves travel at much smaller speeds compared to the speed of modern electronics, therefore, the active cell response can be made virtually instantaneous. In addition, there are well known design techniques and ubiquitous high-quality components for electronic circuits that work at the low frequencies needed in acoustics (typically well under 100 MHz).

As with any active system, the approach presented here has to take into account stability issues. The sensing and driven transducers are typically coupled. The sound produced by one is sensed by the other, which, together with the electronic circuits connecting them form an intracell feedback loop. The electronics have to take this feedback into account in order to maintain the metafluid cell stable. However, this is a typical problem studied in detail in electronic design, which has standard solutions. Moreover, the S-parameter technique used to characterize the metafluid in terms of effective material parameters allows us to use well analyzed methods to take into account intercell interactions and design stable bulk metafluids.

The extended range of achievable effective material parameters enabled by the techniques presented in this article and the tunability of these parameters recommend active metafluids as good candidates for transformation acoustics devices, better performing acoustic lenses, and reconfigurable acoustic devices in general.

ACKNOWLEDGMENT

This work was supported by Grant No. N00014-12-1-0460 from the Office of Naval Research.

*bap7@ee.duke.edu
†cummer@ee.duke.edu

[1] S. A. Cummer and D. Schurig, New J. Phys. **9**, 45 (2007).
[2] H. Chen and C. T. Chan, Appl. Phys. Lett. **91**, 183518 (2007).
[3] S. A. Cummer, B.-I. Popa, D. Schurig, D. R. Smith, J. B. Pendry, M. Rahm, and A. F. Starr, Phys. Rev. Lett. **100**, 024301 (2008).
[4] A. N. Norris, Proc. R. Soc. A **464**, 2411 (2008).
[5] R. S. Lakes, T. Lee, A. Bersie, and Y. C. Wang, Nature (London) **410**, 565 (2001).
[6] J. Li and C. T. Chan, Phys. Rev. E **70**, 055602(R) (2004).
[7] N. Fang, D. Xi, J. Xu, M. Ambati, W. Srituravanich, C. Sun, and X. Zhang, Nature Mater. **5**, 452 (2006).
[8] G. W. Milton, M. Briane, and J. R. Willis, New J. Phys. **8**, 248 (2006).
[9] Y. Ding, Z. Liu, C. Qiu, and J. Shi, Phys. Rev. Lett. **99**, 093904 (2007).
[10] S. Zhang, L. Yin, and N. Fang, Phys. Rev. Lett. **102**, 194301 (2009).
[11] S. H. Lee, C. M. Park, Y. M. Seo, Z. G. Wang, and C. K. Kim, Phys. Rev. Lett. **104**, 054301 (2010).
[12] R. Gracia-Salgado, D. Torrent, and J. Sanchez-Dehesa, New J. Phys. **14**, 103052 (2012).
[13] Z. Liang and J. Li, Phys. Rev. Lett. **108**, 114301 (2012).
[14] Y. Xie, B.-I. Popa, L. Zigoneanu, and S. A. Cummer, Phys. Rev. Lett. **110**, 175501 (2013).
[15] G. W. Milton and J. R. Willis, Proc. R. Soc. A **463**, 855 (2007).
[16] J. B. Pendry and J. Li, New J. Phys. **10**, 115032 (2008).
[17] D. Torrent and J. Sanchez-Dehesa, New J. Phys. **10**, 063015 (2008).
[18] Y. Cheng, F. Yang, J. Y. Xu, and X. J. Liua, Appl. Phys. Lett. **92**, 151913 (2008).
[19] J. Li, L. Fok, X. Yim, G. Bartal, and X. Zhang, Nature Mater. **8**, 931 (2009).
[20] S. Zhang, C. Xia, and N. Fang, Phys. Rev. Lett. **106**, 024301 (2011).
[21] L. Zigoneanu, B.-I. Popa, A. F. Starr, and S. A. Cummer, J. Appl. Phys. **109**, 054906 (2011).
[22] B.-I. Popa, L. Zigoneanu, and S. A. Cummer, Phys. Rev. Lett. **106**, 253901 (2011).
[23] B.-I. Popa and S. A. Cummer, Phys. Rev. B **83**, 224304 (2011).
[24] J. Mei, G. Ma, M. Yang, Z. Yang, W. Wen, and P. Sheng, Nature Commun. **3**, 756 (2012).
[25] B.-I. Popa and S. A. Cummer, Phys. Rev. B **80**, 174303 (2009).
[26] S.-C. S. Lin, T. J. Huang, J. H. Sun, and T. T. Wu, Phys. Rev. B **79**, 094302 (2009).
[27] A. Climente, D. Torrent, and J. Sanchez-Dehesa, Appl. Phys. Lett. **97**, 104103 (2010).
[28] T. P. Martin, M. Nicholas, G. Orris, L. Cai, D. Torrent, and J. Sanchez-Dehesa, Appl. Phys. Lett. **97**, 113503 (2010).
[29] L. Zigoneanu, B.-I. Popa, and S. A. Cummer, Phys. Rev. B **84**, 024305 (2011).
[30] D. Li, L. Zigoneanu, B.-I. Popa, and S. A. Cummer, J. Acoust. Soc. Am. **132**, 2823 (2012).
[31] D. Torrent and J. Sanchez-Dehesa, Phys. Rev. Lett. **108**, 174301 (2012).
[32] T. P. Martin, C. N. Layman, K. M. Moore, and G. J. Orris, Phys. Rev. B **85**, 161103(R) (2012).
[33] W. Akl and A. Baz, J. Intell. Mater. Syst. Struct. **21**, 541 (2010).
[34] W. Akl and A. Baz, J. Appl. Phys. **112**, 084912 (2012).
[35] B.-I. Popa and S. A. Cummer, Microwave Opt. Techn. Lett. **49**, 2574 (2007).
[36] Y. Yuan, B.-I. Popa, and S. A. Cummer, Opt. Express **17**, 16135 (2009).
[37] B.-I. Popa and S. A. Cummer, Phys. Rev. B **85**, 205101 (2012).
[38] D. M. Pozar, *Microwave Engineering* (Wiley, New York, 2004).
[39] V. Fokin, M. Ambati, C. Sun, and X. Zhang, Phys. Rev. B **76**, 144302 (2007).
[40] T. Koschny, P. Markos, D. R. Smith, and C. M. Soukoulis, Phys Rev. E **68**, 065602(R) (2003).
[41] M. L. Edwards and J. H. Sinsky, IEEE Trans. Microwave Theory Tech. **40**, 2303 (1992).
[42] J. B. Pendry, Science **306**, 1353 (2004).
[43] J. B. Pendry, Science **322**, 71 (2008).